

Confinement of Anomalous Liquids in Nanoporous Matrices

Elena G. Strelakova,¹ Jiayuan Luo,¹ H. Eugene Stanley,¹ Giancarlo Franzese,² and Sergey V. Buldyrev³

¹Center for Polymer Studies and Department of Physics, Boston University, Boston, Massachusetts 02215, USA

²Departament de Física Fonamental, Universitat de Barcelona, Diagonal 645, 08028 Barcelona, Spain

³Department of Physics, Yeshiva University, 500 West 185th Street, New York, New York 10033, USA

(Received 3 January 2012; revised manuscript received 29 March 2012; published 4 September 2012)

Using molecular dynamics simulations, we investigate the effects of different nanoconfinements on complex liquids—e.g., colloids or protein solutions—with density anomalies and a liquid-liquid phase transition (LLPT). In all the confinements, we find a strong depletion effect with a large increase in liquid density near the confining surface. If the nanoconfinement is modeled by an ordered matrix of nanoparticles, we find that the anomalies are preserved. On the contrary, if the confinement is modeled by a disordered matrix of nanoparticles, we find a drastically different phase diagram: the LLPT shifts to lower pressures and temperatures, and the anomalies become weaker, as the disorder increases. We find that the density heterogeneities induced by the disordered matrix are responsible for the weakening of the LLPT and the disappearance of the anomalies.

DOI: [10.1103/PhysRevLett.109.105701](https://doi.org/10.1103/PhysRevLett.109.105701)

PACS numbers: 64.70.Ja, 65.20.-w, 66.10.C-

Many experiments in recent years have shown that a number of liquids exhibit highly anomalous properties [1]. The data for liquid metals, metalloids, nonmetals, oxides, and alloys—including Ga, Bi, Te, S, Be, Mg, Ca, Sr, Ba, SiO₂, P, Se, Ce, Cs, Rb, Co, Ge, Ge₁₅Te₈₅—colloids, protein solutions, organophosphates, such as triphenyl phosphite (TPP), AY20 melts [(Al-O)₈₀ - (Y-O)₂₀], and water, reveal the presence of a temperature of maximum density (TMD) below which the density decreases under isobaric cooling [1]. In a number of these systems, such as P, TPP, and AY20 [2], it has been shown that a liquid-liquid phase transition (LLPT) exists and that it ends in a liquid-liquid critical point (LLCP) between two coexisting liquids with the same composition but different structure: the high density liquid (HDL) and the low density liquid (LDL). Data from experiments on silica, C, Se, Co, and water are consistent with a LLPT [3]. Here, we ask how the structure of the nanoconfinement may change the anomalous behavior of the liquid and affect the LLPT and the LLCP. This question is relevant across a wide range of nanotechnological applications, biological systems, and is of general interest for phase transitions in confined systems [4].

We model the liquid using two different potentials, (i) the Jagla ramp potential [5] and (ii) the continuous shoulder potential [6], which reproduce thermodynamic and dynamic anomalies, LLPT and LLCP in bulk. We model the nanoconfinement by a fixed matrix of nanoparticles (NPs) connected by bonds which the liquid particles can penetrate. Potential (i) has a hard-core at distance $r = a$, and a linear ramp for $a < r \leq b$ decreasing from interaction energy $U_R > 0$ to $-U_0 < 0$, plus a linear ramp for $b < r \leq c$ increasing from $-U_0$ to 0. We adopt $b/a = 1.72$, $c/a = 3$, and $U_R = 3.56U_0$. The liquid particles interact with NPs via hard-core repulsion at distance $r_0 \equiv (a + D_{\text{NP}})/2$, where D_{NP} is the NP diameter. Potential

(ii) has a repulsive shoulder and an attractive well with energy minimum U_0 , with parameters chosen to fit a potential proposed in Ref. [7]. The interaction with NPs is given by a $1/(r - r_0)^{100}$ power law.

For both potentials, we perform simulations at constant number N of liquid particles, constant volume V , and constant temperature T , with periodic boundary conditions. For (i), we employ a discrete molecular dynamics (MD) algorithm by discretizing the linear ramp potential into steps, with $\Delta U \equiv U_0/8$ [8]. For (ii), we use a standard MD with a velocity Verlet integrator and the Allen thermostat [6].

We consider three different structures for the matrix: a perfect cubic lattice (CUBE); a cubic lattice with Gaussian distortions (DIST) with a standard deviation equal to 1/4th the separation between centers of NPs, which still preserves an approximately periodic and ordered structure of the confinement [Fig. 1(a)]; and a completely random (RND) configuration of NPs obtained by simulating a gas of hard spheres [Fig. 1(b)]. The volume fraction of NPs is $x_{\text{NP}} \equiv V_{\text{NP}}/V$, where V is the volume of the cubic simulation box and $V_{\text{NP}} = N_{\text{NP}}4\pi r_0^3/3$ is the volume inaccessible to the liquid. Our results here, if not otherwise indicated, are for liquid (i) confined by the matrix of $N_{\text{NP}} = 64$ NPs with diameter $D_{\text{NP}}/a = 3$ at $x_{\text{NP}} = 24.5\%$ and $V/a^3 = 20.6^3$. We control the density $\rho \equiv N/(V - V_{\text{NP}})$ of the liquid particles by changing N in the interval between 1845 and 3887. We take into account that the excluded volume rescales the pressure P by $V/(V - V_{\text{NP}})$. We find that the results for liquid (ii) are consistent in similar conditions.

For liquid (i), the bulk system displays a LLCP at $k_B T_c^{\text{bulk}}/U_0 = 0.375$, $P_c^{\text{bulk}} a^3/U_0 = 0.243$, and $\rho_c^{\text{bulk}} a^3 = 0.37$ [5]. Figures 1(c) and 1(d) show simulated isochores for DIST and RND confinement, respectively, with the

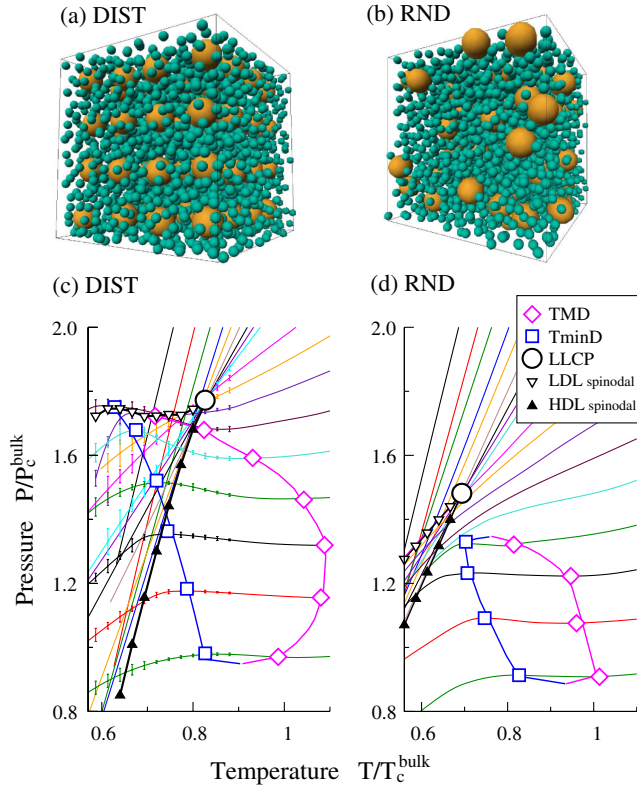


FIG. 1 (color online). Effect of confinement. Snapshots of the anomalous liquid (green, small spheres) confined in a fixed matrix of NPs (yellow, large spheres) in a DIST (a) and RND (b) configuration. Polynomial fits of simulated isochores of densities $0.89 \leq \rho/\rho_c^{\text{bulk}} \leq 1.59$ (bottom to top in the one-phase region) for DIST (c) and RND (d). Randomness reduces the temperature and pressure of the LLC (circles), the separation between the HDL (lower filled triangles) and LDL spinodals (upper open triangles), and the separation between the TMD (diamonds) and the temperature of minimum densities (TminD, squares). Samples of error bars on P are given in panel (c). Lines connecting symbols are guides for the eyes.

HDL-LDL spinodal lines calculated using conditions $(\partial P/\partial \rho)_T = 0$ and $(\partial^2 P/\partial \rho^2)_T \neq 0$ [9], and the LLC obtained at the point of merging of the spinodal lines, where $(\partial P/\partial \rho)_T = (\partial^2 P/\partial \rho^2)_T = 0$. We find that every confinement causes the LLC to shift to a lower T , a higher ρ , and a higher P than in the bulk liquid [Fig. 2(a)]. As the disorder in the confining matrix increases, the T shift is more pronounced and the ρ and P shifts less pronounced. We find the same qualitative trend in the LLC shifts for liquid (ii), and that the LLC progressively approaches the bulk case when the NP concentration decreases [Fig. 2(b)], consistent with previous results for NP-liquid mixtures [10].

While the periodic DIST confinement preserves the LDL-HDL coexistence region observed in bulk liquid [Fig. 1(c)], which is consistent with a strong first-order LLPT, the RND confinement shrinks the coexistence region [Fig. 1(d)] and weakens at the LLPT, which

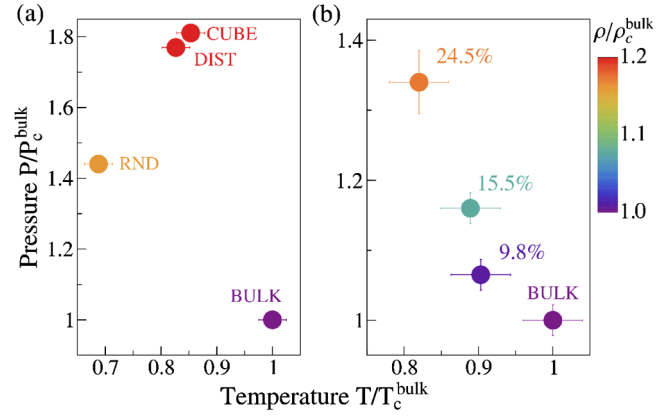


FIG. 2 (color online). The effect of different confinements on the parameters of the LLC. Color coded circles (from dark blue for lower ρ to bright red for higher ρ) represent the LLC parameters in the $P-T-\rho$ phase space (a) for the liquid confined in the fixed matrix of NPs with CUBE, DIST, and RND configuration. Increasing disorder in the confinement, from CUBE to DIST to RND, shifts the LLC down in ρ , T , and P . (b) Upon decreasing concentration x_{NP} (label near the symbols) for the CUBE confinement of the liquid (ii), the LLC approaches the bulk case. Here, we use $N_{\text{NP}} = 64$ NPs with $D_{\text{NP}}/a = 3$ in $V/a^3 = 20.6^3$ at $x_{\text{NP}} = 24.5\%$ with $1452 \leq N \leq 2508$ (with spontaneous crystallization below the LLC), or in $V/a^3 = 24^3$ at $x_{\text{NP}} = 15.5\%$ with $2570 \leq N \leq 4439$, or in $V/a^3 = 28^3$ at $x_{\text{NP}} = 9.8\%$ with $4358 \leq N \leq 7528$. We find the same behavior for liquid (i). The models of liquid with two potentials (i) and (ii) are described in the text.

manifests itself in the shrinking of the region between the spinodals in the $P-T$ plane. This shrinking is qualitatively consistent with that found for a model of water in a random hydrophobic pore-like confinement [11].

The region of density anomaly is bounded by the lines of the TMD and the temperature of minimum density (TminD) located by the extrema of the isochores. In the bulk system, the TminD line for high densities is hindered by the glass temperature line and cannot be observed in the equilibrium liquid. Here, we observe that the periodic structure of the confinement can dramatically affect density anomaly manifestations. Compared to the bulk, confinement decreases TMD and increases TminD, shrinking the T range of the density anomaly. The density anomaly is still well-defined in the DIST case, but it appears much less pronounced in the RND case. For a RND matrix of $N_{\text{NP}} = 19$ large confining NPs with diameter $D_{\text{NP}}/a = 5$ at $x_{\text{NP}} = 24.5\%$ and $V/a^3 = 20.6^3$, the TMD and TminD are completely absent (not shown).

To understand the origin of the different effects of the different confinements, we study the density of the liquid in the vicinity of NPs. We find that a layer of liquid adsorbs onto the NPs, as revealed by the fluid density profile $g_{\text{NP-liq}}(r)$ (Fig. 3). We understand the increase of density near the NP surface as a consequence of entropy maximization. By packing near the fixed NPs, the adsorbed

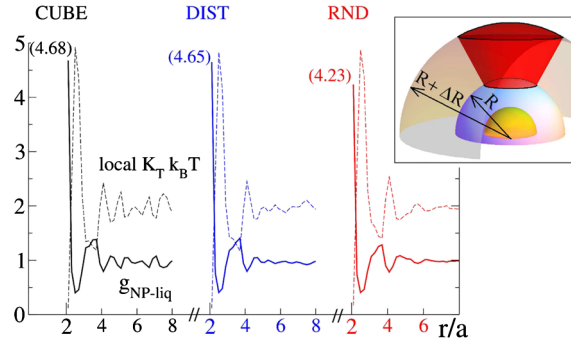


FIG. 3 (color online). The liquid adsorbs onto the NPs. The fluid density profile $g_{\text{NP-liq}}(r)$ at $T/T_c^{\text{bulk}} = 1.12$ for CUBE (leftmost), DIST (center), and RND (rightmost) confinements for the density $\rho/\rho_c^{\text{bulk}} = 1.59$ (solid lines) display large maxima (values in parenthesis) at the closest NP-liquid particle distance $r = r_0 \equiv 2a$. Local compressibility K_T (dashed lines) shows large peaks near the minimum of $g_{\text{NP-liq}}(r)$. The results for different confinements are shifted horizontally for clarity. Inset: Schematic representation of calculation of $g_{\text{NP-liq}}(r)$ and local K_T inside equal-volume ($\Delta W = 2.77a^3$) conical regions between two concentric spheres with different radii R and $R + \Delta R$ centered at the NP (small yellow hemisphere in the middle), where $\Delta R = 0.2a$ and $R = 2.0a, 2.2a, \dots, 8.0a$ (one such conical region is shown in dark red). The axis of the conical region is chosen at random 10 000 times for each NP. $g_{\text{NP-liq}}(r)$ is computed by counting the number of liquid particles and local $K_T = [(\langle n^2 \rangle / \langle n \rangle^2) - 1](\Delta W / k_B T)$ from fluctuations of number of liquid particles n .

liquid particles allow more free space to the the rest of the liquid, maximizing the entropy of the system (depletion effect). This result evokes a similar effect found for water at confining surfaces, regardless of the hydrophobic or hydrophilic interaction with the surface [12], and for hard-sphere fluids in contact with purely repulsive particles [13], showing that the increase of contact density is not related to specific interactions or anomalous behaviors and making a bridge between water and simple fluids.

We find that, by increasing randomness in the confinement, the probability of overlap of NP exclusion volumes increases and the depletion effect decreases. As a consequence, the density of liquid near the NPs decreases (Fig. 3). In addition, we analyze the density fluctuations and the associated measurable response function, the local isothermal compressibility K_T (Fig. 3), of the liquid in the vicinity of the NPs. We find that K_T is extremely small at the interface, consistent with a tight packing of liquid particles around the NPs. Near the first minimum of $g_{\text{NP-liq}}(r)$, K_T is, instead, twice as high as in the bulk. A high local density causes the density increase of the LLC (Fig. 2) because, when part of the liquid is adsorbed onto the NPs, an average liquid density larger than bulk is necessary to build up the critical fluctuations. The shift is more pronounced for CUBE and DIST confinement, with respect to RND, because the more ordered the

confinement, the larger the NP surface available for the depletion effect.

To better understand how confinement structure affects the physical properties of a liquid, we study the liquid's local density distribution inside the confinement matrix. We identify the region not occupied by the NPs and partition it into disconnected *cavities* [inset Fig. 4(c)] based on the Delaunay tessellation algorithm described in Ref. [14]. We define the exclusion spheres concentric with NPs and gradually increase their radius r_e with a small step $\Delta r_e = 0.1a$. We designate the space not occupied by exclusion spheres as *void* of size r_e and denote it $\Omega(r_e)$. For

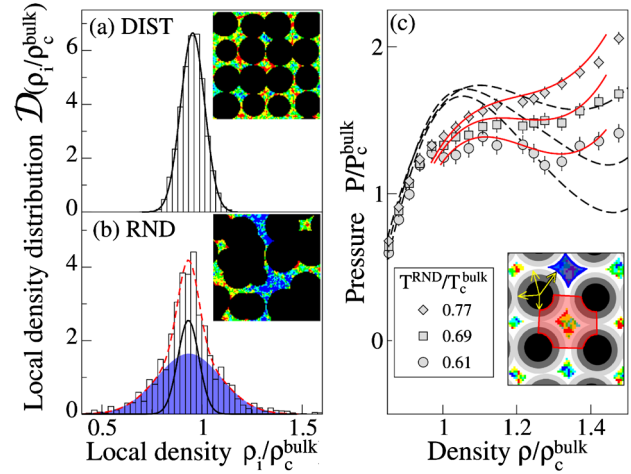


FIG. 4 (color online). The distribution of local density $\mathcal{D}(\rho_i/\rho_c^{\text{bulk}})$ of the liquid inside the pockets for global liquid density $\rho/\rho_c^{\text{bulk}} = 0.94$ and $T/T_c^{\text{bulk}} = 0.88$. (a) In the DIST confinement, at $P/P_c^{\text{bulk}} = 1.3$, $\mathcal{D}^{\text{DIST}}(\rho_i/\rho_c^{\text{bulk}})$ is a Gaussian centered at $\rho/\rho_c^{\text{bulk}} = 0.94$ with standard deviation $\sigma_D = 0.055$. Inset: Cut through the simulation box. The liquid density (high to low color coded from blue to red) is computed inside spheres of radius $1.5a$ that do not intersect NPs. Areas for which we cannot evaluate liquid density with this method are in black. (b) In RND confinement, at $P/P_c^{\text{bulk}} = 1.25$, the broad $\mathcal{D}^{\text{RND}}(\rho_i/\rho_c^{\text{bulk}})$ (red dashed line) is the result of two Gaussian components, both centered in $\rho/\rho_c^{\text{bulk}} = 0.94$, but with different standard deviations: one is due to the local density fluctuations (black line) with $\sigma_{R1} = 0.052$, as in DIST, and the other with $\sigma_{R2} = 0.159$ (shaded) due to the heterogeneity in pockets volumes. Inset: As in panel (a), but for RND. (c) Calculation of P^{RND} by taking into account the component of $\mathcal{D}^{\text{RND}}(\rho_i/\rho_c^{\text{bulk}})$ due to the heterogeneity in pocket volumes. Polynomial fits of the isotherms, $P^{\text{DIST}}(\rho)$ at constant T (black dashed lines: from top to bottom $T/T_c^{\text{bulk}} = 0.77, 0.69, 0.61$), are used in Eq. (1) to get an estimate of $P^{\text{RND}}(\rho)$ at the same T (red solid lines), which compare well, within a range of densities close to the LLPT, with the simulation data for RND (symbols). Inset: 2D representation of the exclusion spheres (black, grey, white circles) with their radii r_e (yellow arrows), which for $r_e = r_0$ (black circles) coincides with NPs. A cavity is shown as a blue diamond and a pocket is shown as a red square-like segment. For clarity, the liquid (colored regions) is shown inside cavities only.

$r_e = r_0$, $\Omega(r_0)$ is a connected set for both RND and DIST confinements. The volume of $\Omega(r_0)$ is equal to $V - V_{\text{NP}}$.

In DIST confinement, when $r_e > 4.1a$, $\Omega(r_e)$ breaks into 64 small disconnected cavities, associated with 64 distorted cubic *pockets* formed by 8 adjacent NPs. The volume ω_i of each pocket $i = 1, \dots, 64$ is given by the volume of all Delaunay tetrahedra comprising the corresponding pocket minus the volume occupied by the NPs forming the pocket. We define the particle density of liquid in each pocket $\rho_i \equiv N_i/\omega_i$, where N_i is the number of liquid particles inside pocket i . We find that the volumes ω_i are narrowly distributed, with the local liquid density distribution $\mathcal{D}^{\text{DIST}}(\rho_i)$ given by a Gaussian with variance σ_D^2 [Fig. 4(a)].

In RND confinement, $\Omega(r_e)$ remains fully connected up to $r_e = 4.2a$. As we increase r_e , small pockets break away from the largest part of $\Omega(r_e)$ one by one. When $r_e = 5.4a$, we count, for different random configurations, approximately 60 pockets, for which we calculate ω_i and ρ_i , finding a large variety of sizes and shapes. We compute $\mathcal{D}^{\text{RND}}(\rho_i)$ and find that in RND it can be approximated with the sum of two Gaussian distributions: one similar to the DIST case with $\sigma_{R1} \approx \sigma_D$ and the other resulting from the heterogeneity of volumes ω_i of the pockets with $\sigma_{R2} > \sigma_{R1}$ [Fig. 4(b)].

We hypothesize that in RND confinement, the observed pressure $P^{\text{RND}}(T, \rho)$ results from averaging local pressures in each pocket. At temperature T , we estimate P^{RND} using the average of the $P^{\text{DIST}}(T, \rho_i)$ over all heterogeneous pockets [Fig. 4(c)],

$$P^{\text{RND}}(T, \rho) = \int P^{\text{DIST}}(T, \rho + \rho\xi) \frac{\exp[-\xi^2/2\sigma_{R2}^2]}{\sqrt{2\pi\sigma_{R2}^2}} d\xi. \quad (1)$$

Due to averaging over different densities $\rho_i \equiv \rho + \rho\xi$, the nonmonotonic subcritical isotherm $P^{\text{DIST}}(\rho)$ at $T = T_c^{\text{RND}} < T_c^{\text{DIST}}$ becomes a monotonic critical isotherm $P^{\text{RND}}(\rho)$ that closely fits the simulation results for the RND confinement in the vicinity of the LLPT. Thus, our averaging technique allows us to reproduce quantitatively the differences we found when we compared DIST and RND confinements; i.e., the critical temperature, pressure, and density decrease [Fig. 2(a)] and density anomaly region shrinks [Figs. 1(c) and 1(d)]. Thus, the presence of density heterogeneity and the reduced depletion effect in the RND confinement matrix give us the key to understanding the effect of confinement structures. It is important to stress the differences of the effect of confinement on the LLPT and the liquid-gas phase transition (LGPT). While in both cases the critical temperature is significantly reduced, the effects of random confinement and ordered confinement are practically indistinguishable in the case of LGPT. This is because in LGPT, the density of liquid particles has a much smaller increase near NPs than in

LLPT. Thus, in LGPT, randomness does not lead to local density heterogeneities, which produce a strong effect on the LLPT.

In conclusion, we predict that anomalous liquids with a LLPT retain their bulk phase diagram and density anomalies when they are confined in a porous matrix with an ordered structure. Furthermore, when there is a small distortion of the confinement, the glass temperature is reduced with respect to bulk, allowing the direct observation of the TminD locus. A strong depletion effect induces a large increase of density in the vicinity of the NPs. The effect is smaller when the confinement has a random structure. Randomness induces heterogeneity in the local density, which weakens the LLPT, narrows the LLPT coexistence region, and washes out the density anomalies.

Although the anomalous liquids considered here are, in principle, different from water, our results could qualitatively explain recent experiments for confined water, the prototypical anomalous liquid. While the TminD locus has been observed in supercooled water under hydrophilic confinement by the MCM-41 silica nanoporous matrix [15], its absence has been reported in the hydrophobic mesoporous material CMK [16]. MCM-41 forms a regular matrix [15], but CMK consists of grains, each with a disordered pore structure [16]. This suggests that the disparity of results for different confinements may arise from the different amount of disorder in the confining structures, independent of the interaction details of the anomalous liquid.

We thank D. Corradini, P. Gallo, S. Sastry, and K. Stokely for discussions. E. G. S., J. L., and H. E. S. acknowledge the support of NSF Grants No. CHE0908218, No. CHE0911389, and No. CHE1213217. S. V. B. acknowledges the Dr. Bernard W. Gamson Computational Science Center at Yeshiva College, G. F. acknowledges the MICINN Grant No. FIS2009-10210 (co-financed FEDER) and the EU FP7 Grant No. NMP4-SL-2011-266737, S. V. B. and G. F. thank AGAUR Grant No. 2009PIV45.

-
- [1] P. Vilaseca and G. Franzese, *J. Non-Cryst. Solids* **357**, 419 (2011), and references therein.
 - [2] Y. Katayama, T. Mizutani, W. Utsumi, O. Shimomura, M. Yamakata, and K.-i. Funakoshi, *Nature (London)* **403**, 170 (2000); Y. Katayama, Y. Inamura, T. Mizutani, M. Yamakata, W. Utsumi, and O. Shimomura, *Science* **306**, 848 (2004); G. Monaco, S. Falconi, W. A. Crichton, and M. Mezouar, *Phys. Rev. Lett.* **90**, 255701 (2003); H. Tanaka, R. Kurita, and H. Matakai, *ibid.* **92**, 025701 (2004); R. Kurita and H. Tanaka, *Science* **306**, 845 (2004); *J. Phys. Condens. Matter* **17**, L293 (2005); G. N. Greaves *et al.*, *Science* **322**, 566 (2008).
 - [3] C. A. Angell, S. Borick, and M. Grabow, *J. Non-Cryst. Solids* **205–207**, 463 (1996); D. J. Lacks, *Phys. Rev. Lett.* **84**, 4629 (2000); M. van Thiel and F. H. Ree, *Phys. Rev. B* **48**, 3591 (1993); V. V. Brazhkin, E. L. Gromnitskaya, O. V.

- Stal'gorova, and A. G. Lyapin, *Rev. High Pres. Sci. Tech.* **7**, 1129 (1998); M. G. Vasin and V. I. Ladýanov, *Phys. Rev. E* **68**, 051202 (2003); S. Aasland and P. F. McMillan, *Nature (London)* **369**, 633 (1994); M. C. Wilding and P. F. McMillan, *J. Non-Cryst. Solids* **293–295**, 357 (2001).
- [4] F. Detcheverry, E. Kierlik, M. L. Rosinberg, and G. Tarjus, *Phys. Rev. E* **72**, 051506 (2005); N. M. Barraz Jr., E. Salcedo, and M. C. Barbosa, *J. Chem. Phys.* **131**, 094504 (2009); E. Salcedo, A. B. de Oliveira, N. M. Barraz Jr., C. Chakravarty, and M. C. Barbosa, *J. Chem. Phys.* **135**, 044517 (2011).
- [5] E. A. Jagla, *Phys. Rev. E* **63**, 061501 (2001); L. Xu, P. Kumar, S. V. Buldyrev, S.-H. Chen, P. H. Poole, F. Sciortino, and H. E. Stanley, *Proc. Natl. Acad. Sci. U.S.A.* **102**, 16558 (2005); L. Xu, S. V. Buldyrev, C. A. Angell, and H. E. Stanley, *Phys. Rev. E* **74**, 031108 (2006); *J. Chem. Phys.* **130**, 054505 (2009); L. Xu, S. V. Buldyrev, N. Giovambattista, C. A. Angell, and H. E. Stanley, *J. Chem. Phys.* **130**, 054505 (2009).
- [6] G. Franzese, *J. Mol. Liq.* **136**, 267 (2007); A. B. de Oliveira, G. Franzese, P. A. Netz, and M. C. Barbosa, *J. Chem. Phys.* **128**, 064901 (2008); P. Vilaseca and G. Franzese, *ibid.* **133**, 084507 (2010).
- [7] T. Head-Gordon and F. H. Stillinger, *J. Chem. Phys.* **98**, 3313 (1993).
- [8] S. V. Buldyrev, *Lect. Notes Phys.* **752**, 97 (2008).
- [9] See Supplemental Material at <http://link.aps.org/supplemental/10.1103/PhysRevLett.109.105701> for details on the determination of the LLCP.
- [10] D. Corradini, S. V. Buldyrev, P. Gallo, and H. E. Stanley, *Phys. Rev. E* **81**, 061504 (2010).
- [11] E. G. Strelakova, M. G. Mazza, H. E. Stanley, and G. Franzese, *Phys. Rev. Lett.* **106**, 145701 (2011).
- [12] I. V. Brovchenko, A. Geiger, and D. Paschek, *Fluid Phase Equilib.* **183–184**, 331 (2001); T. Werder, J. H. Walther, R. L. Jaffe, T. Halicioglu, and P. Koumoutsakos, *J. Phys. Chem. B* **107**, 1345 (2003); P. Kumar, S. V. Buldyrev, F. W. Starr, N. Giovambattista, and H. E. Stanley, *Phys. Rev. E* **72**, 051503 (2005); J. Marti, G. Nagy, M. C. Gordillo, and E. Guàrdia, *J. Chem. Phys.* **124**, 094703 (2006); G. Cicero, J. C. Grossman, E. Schwegler, F. Gygi, and G. Galli, *J. Am. Chem. Soc.* **130**, 1871 (2008); R. Godawat, S. N. Jamadagni, and S. Garde, *Proc. Natl. Acad. Sci. U.S.A.* **106**, 15119 (2009).
- [13] P.-M. König *et al.*, *Europhys. Lett.* **69**, 832 (2005).
- [14] S. Sastry, D. S. Corti, P. G. Debenedetti, and F. H. Stillinger, *Phys. Rev. E* **56**, 5524 (1997).
- [15] F. Mallamace *et al.*, *Proc. Natl. Acad. Sci. U.S.A.* **104**, 18387 (2007).
- [16] Y. Zhang *et al.*, *J. Phys. Chem. B* **113**, 5007 (2009).